Supplementary material for

Drivers of net community production in the bottom of Arctic pack ice

*Rosalie McKay[1], Zoe Koenig[1], Polona Itkin[2], Rolf Gradinger[1], Christien Laber[1], Janina Osanen[3], Sanna Saur Heiland[1], Karley Campbell[1]

[1]Department of Arctic and Marine Biology, UiT The Arctic University of Norway, Tromsø, Norway
[2]Norwegian Polar Institute, Tromsø, Norway
[3]Department of Biology, Norwegian University of Science and Technology, Trondheim, Norway

*corresponding author: rosalie.d.mckay@uit.no

Contents

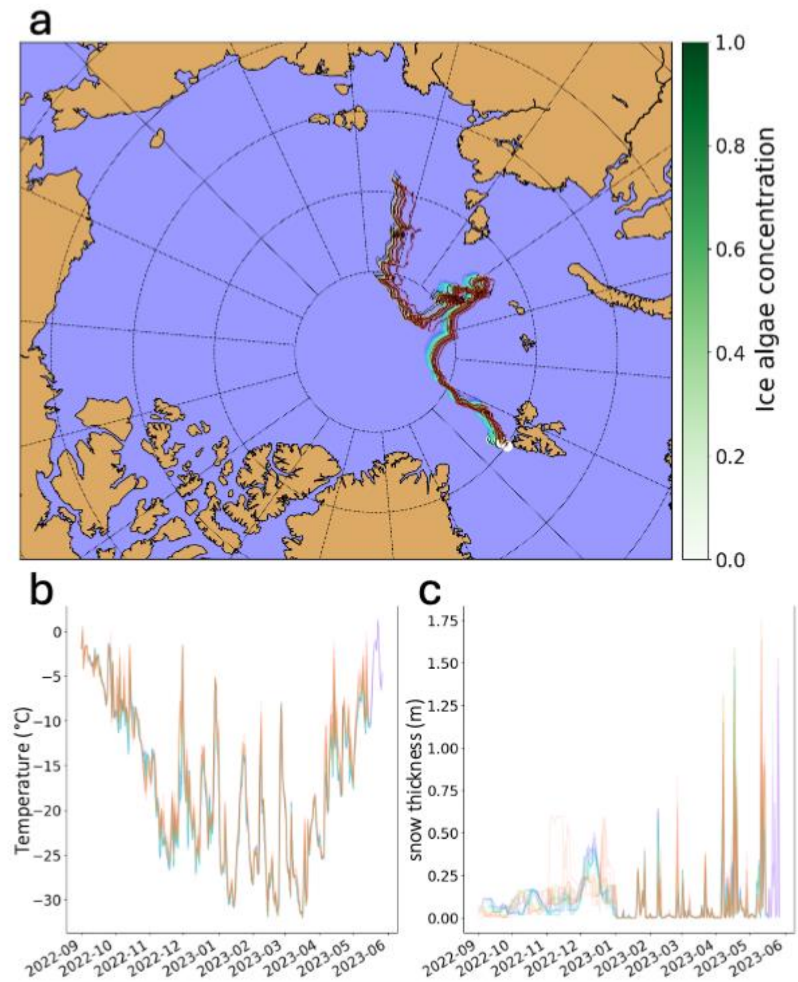

Figure S1: Environmental and Dynamic Evolution of the Study Floe. (a) Back trajectories of the oldest ice associated with each Arctic Shipborne Sea Ice Standardization Tool (ASSIST) observation made during the transit through the ice. Ice algal concentrations were estimated from ASSIST and calculated as a partial-concentration-weighted average of the two observed ice types, $(C_1p_1+C_2p_2)$/total ice concentration, where C_1 and C_2 denote the maximum observed algal concentration associated with each ice type and can take the values of 0, 0.3, 0.6, or 0.9. Panels show time series of (b) mean air temperatures (spikes are storms), and (c) accumulated snowfall along the back trajectories shown in panel (a). Environmental variables were derived from ERA5 reanalysis and satellite-based sea-ice products (Copernicus Climate Change Service (C3S), 2023; Hersbach et al., 2020). Back trajectories were calculated using the SIDRiFT algorithm as described below.

Back trajectory calculation: Following the method described by (Lenss et al., 2025), the provenance of the oldest ice present at each ASSIST observation site was estimated using backward sea-ice trajectories generated with the SIDRiFT algorithm (https://github.com/loniitkina/sidrift). The model uses OSI SAF sea-ice drift (Ocean and Sea Ice Satellite Application Facility (OSI SAF), 2010) and concentration data (Ocean and Sea Ice Satellite Application Facility (OSI SAF), 2017) to reconstruct ice motion through time. Starting from the location and date of each observation, trajectories were propagated backward using daily drift fields derived from the nearest grid point within 100 km. Calculations were discontinued when sea-ice concentration fell below 15 % or when the required input data were unavailable.

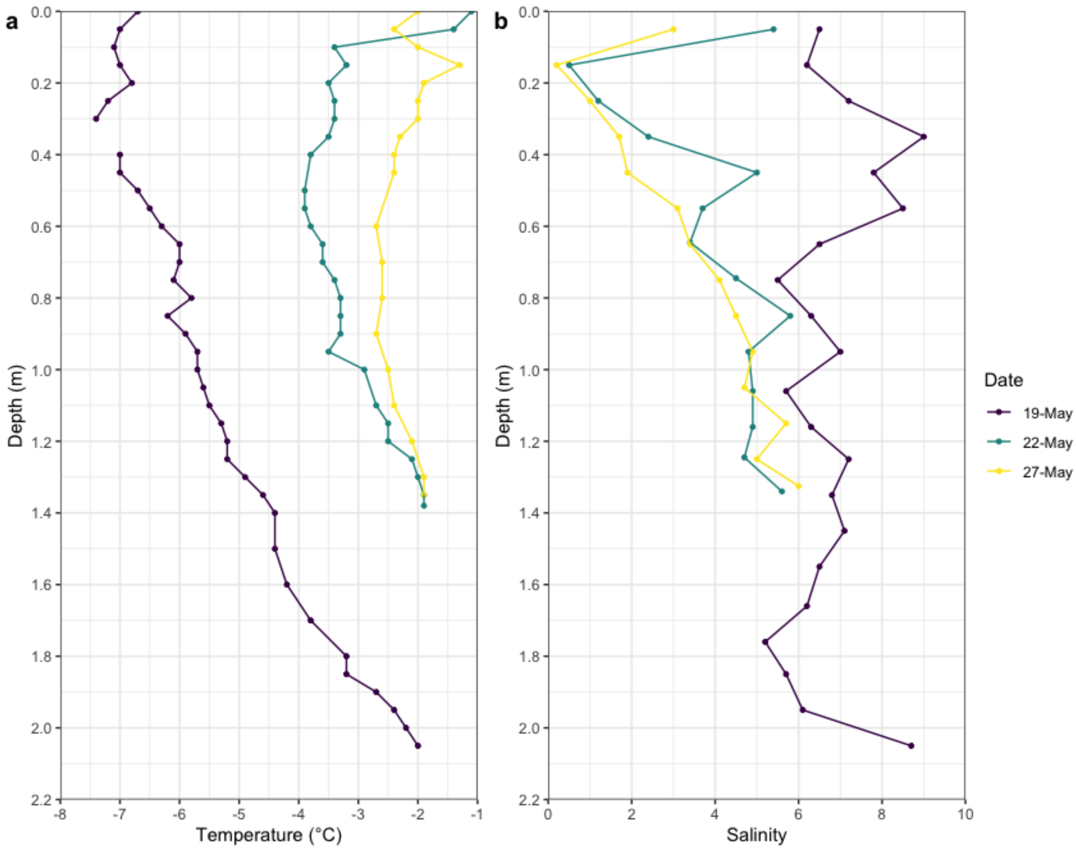

Figure S2: Temperature and salinity profiles of the sea-ice sampling sites. Temperature (a) and salinity (b) of ice column at the sampling sites. The snow ice interface is at 0 m. The cores sampled on 22 May were taken from the thick snow site and covered by 30 cm of snow.

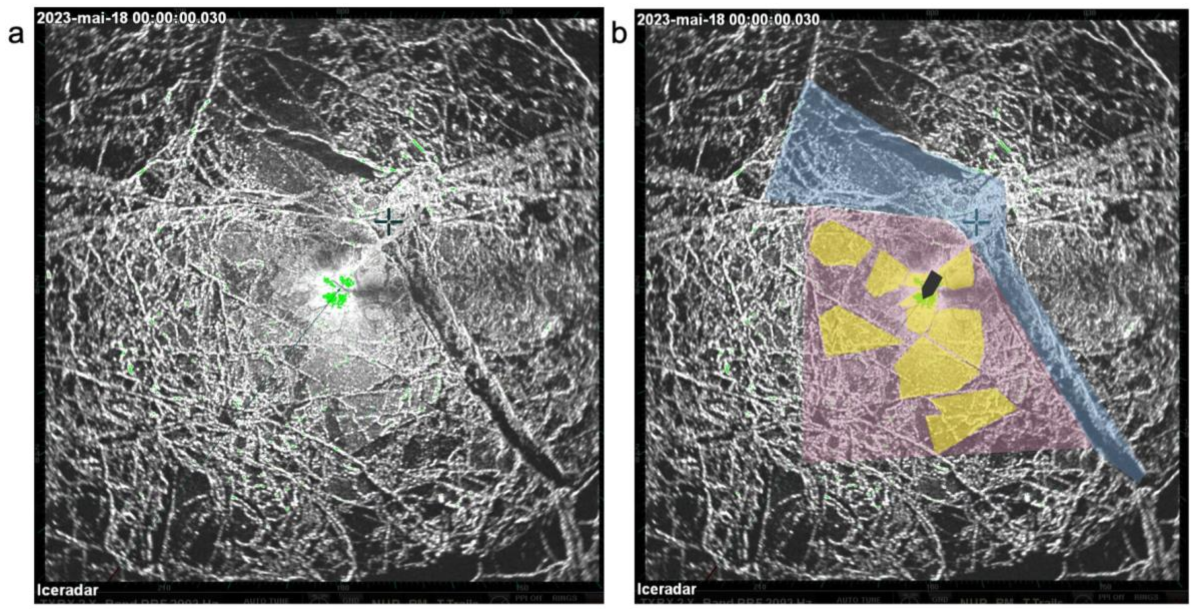

Figure S3: Radar images of the study region (a) Intensity radar image from SHN-X12 (SeaHawk Navigation, X-Band 12ft antenna) showing surface roughness as detected by X-band microwave reflection. Smooth (and saline) areas are dark while rough and desalinated areas are bright. The ship is in the center of the image (black ship symbol). (b) Interpreted ice radar image with second-year ice (SYI) marked as yellow, first-year ice (FYI) as magenta and leads as blue. The ship symbol is not to scale and appears larger for visualization. The lead region features small broken up ice floes and brash ice, resulting in bright features across the lead region.

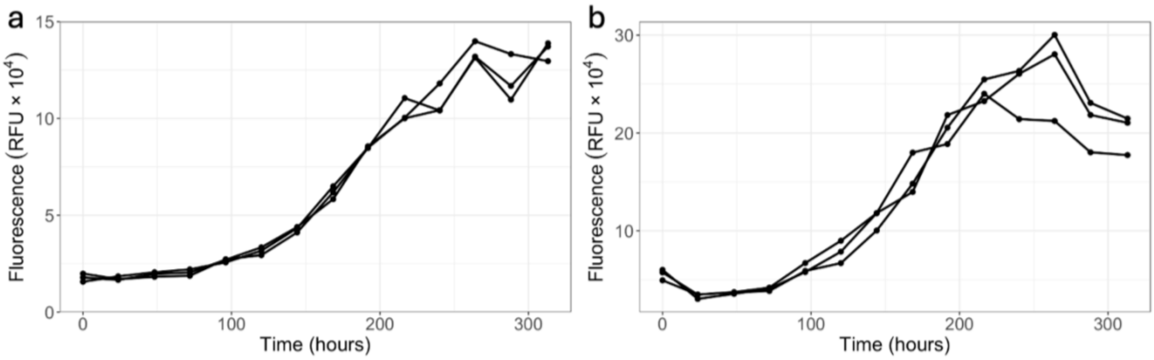

Figure S4: Laboratory algal culture growth curves. Growth curves in raw fluorescence units (RFU) in triplicate for single species cultures of (a) *Nitzschia frigida* and (b) *Pseudonitzschia sp.* Used for laboratory experiments.

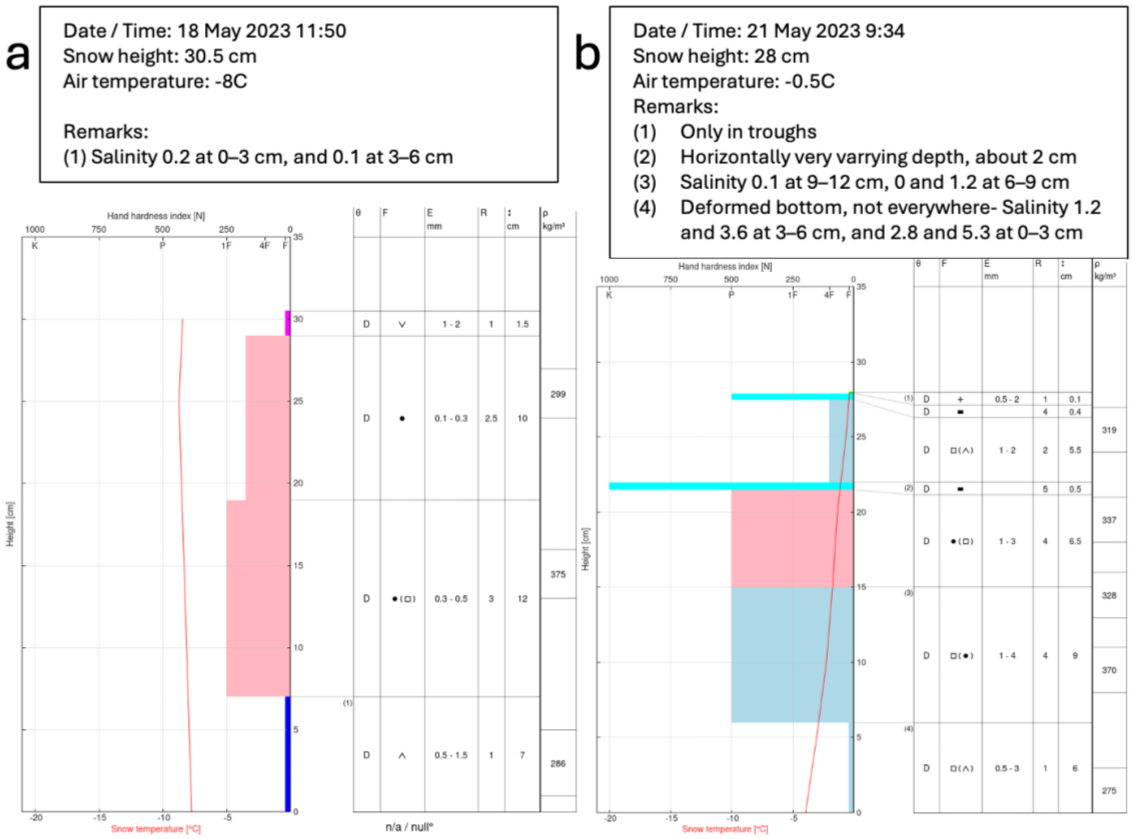

Figure S5: Snow pits over first- and second-year ice of the study sites. (a) Snow pit from first-year ice (FYI) site showing a very simple snow structure of winter snow pack that likely accumulated in low precipitation environment with no significant warm air intrusions. This pit was in a 0.3 m deep snowbank, which was deeper than the average FYI snow thickness based on the transects. A shallower snow pit was not analyzed. (b) Snow pit from second-year ice (SYI) site showing a complex snow structure of snowpack that likely started to accumulate already before sea ice freeze-up and experienced several warm air intrusions in the beginning of the winter. The top section of the snow cover is similar to the FYI snow profile in (a).

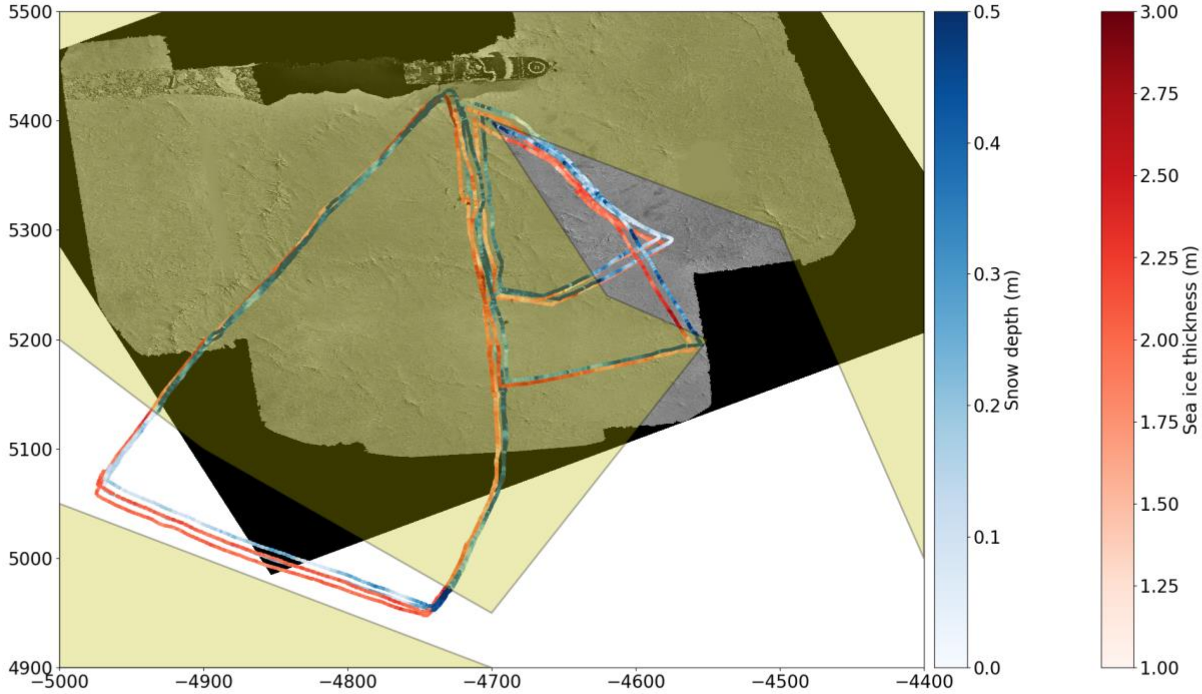

Figure S6: Snow and ice thickness transects. Orthophoto mosaic with snow depth and ice thickness transect data from 18, 21, 24 and 27 May 2023. The tracks are not repeated strictly. SYI area is in yellow (as determined based on the radar image above). The remaining area is FYI. The background is an orthophoto mosaic from drone image taken on 24 May. Regions of black and white fall outside of the drone image (no data).

Table S1: Average snow depth and ice thickness per ice-age class from transects

	Second-year ice			First-year ice		
	Ice thickness (m)	Ice thickness mode (m)	Snow depth (m)	Ice thickness (m)	Ice thickness mode (m)	Snow depth (m)
18 May	1.8±0.3	1.65	0.47±0.19	2.0±0.2	2.05	0.20±0.10
21 May	2.0±0.1	1.85	0.44±0.16	2.0±0.1	2.05	0.19±0.11
24 May	2.1±0.3	1.65	0.42±0.17	2.2±0.1	1.95	0.18±0.11
27 May	2.0±0.3	1.85	0.48±0.20	2.0±0.3	1.75	0.31±0.14

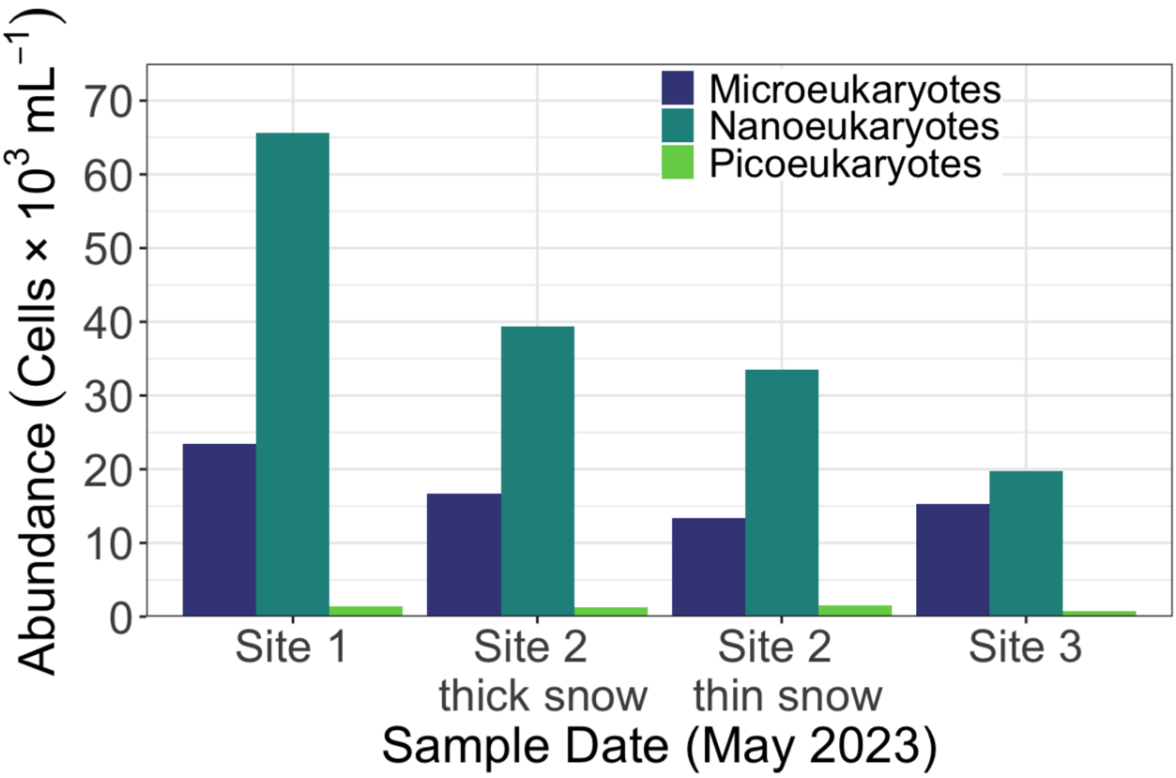

Figure S7: Photosynthetic eukaryote abundances in the bottom ice. (a) Algal abundances in three size classes in the bottom ice. Microeukaryotes were determined by light microscopy and photosynthetic pico- and nanoeukaryotes by flow cytometry.

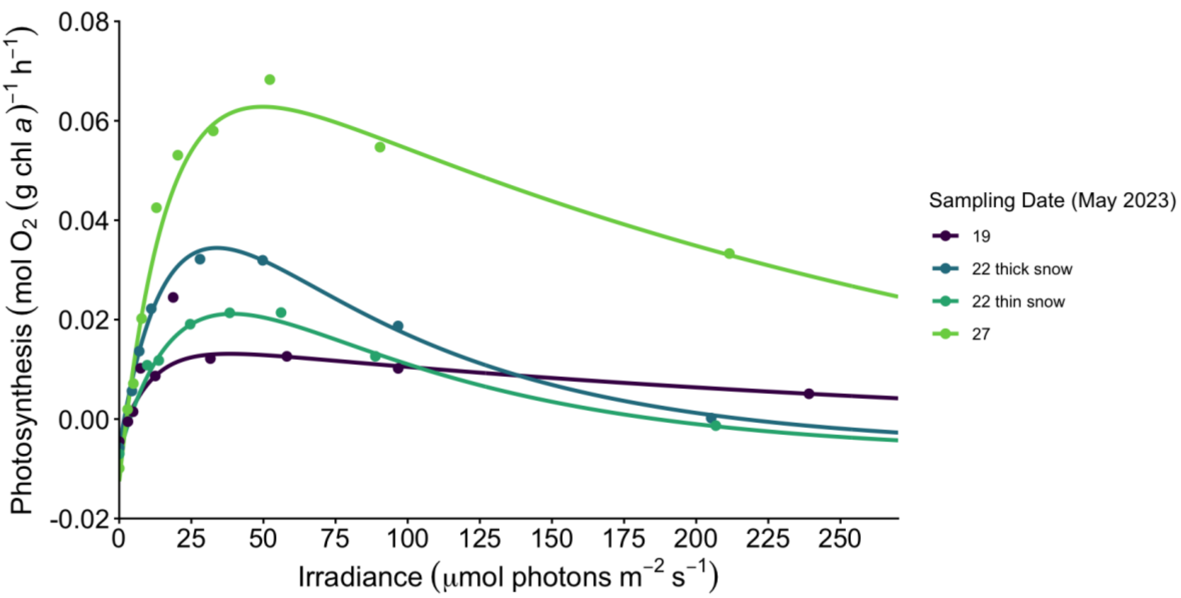

Figure S8: Photosynthesis-Irradiance curves of net community production of the bottom ice.

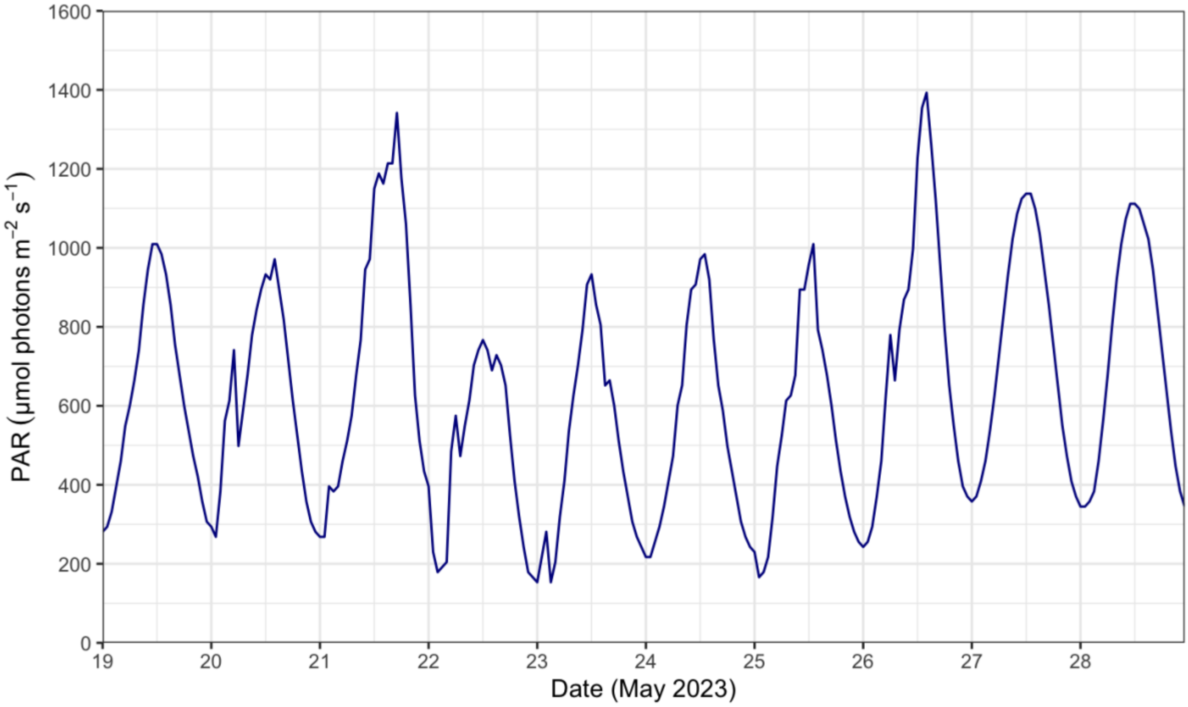

Figure S9: Modelled downwelling irradiance in the PAR range over the sampling period. Obtained from hourly All Sky Surface Total PAR (MJ m^{-2} hr^{-1}) data (NASA Langley Research Center's Prediction Of Worldwide Energy Resources (POWER), version 2.5.22).

Table S2: Under ice transmittance calculated from in situ upwelling and downwelling irradiance in the PAR range

Date / Time	Snow depth (m)	Average Downwelling (µmol photons m^{-2} s^{-1})	Under-ice transmittance (%)
19.05.2023 / 14:00	0.15	812.2 ± 5.4	1.14
22.05.2023 / 10:00	0.28	545.5 ± 0.3	0.64
22.05.2023 / 11:00	0.16	591.3 ± 5.6	0.68
27.05.2023 / 14:00	0.17	843.7 ± 0.4	2.56

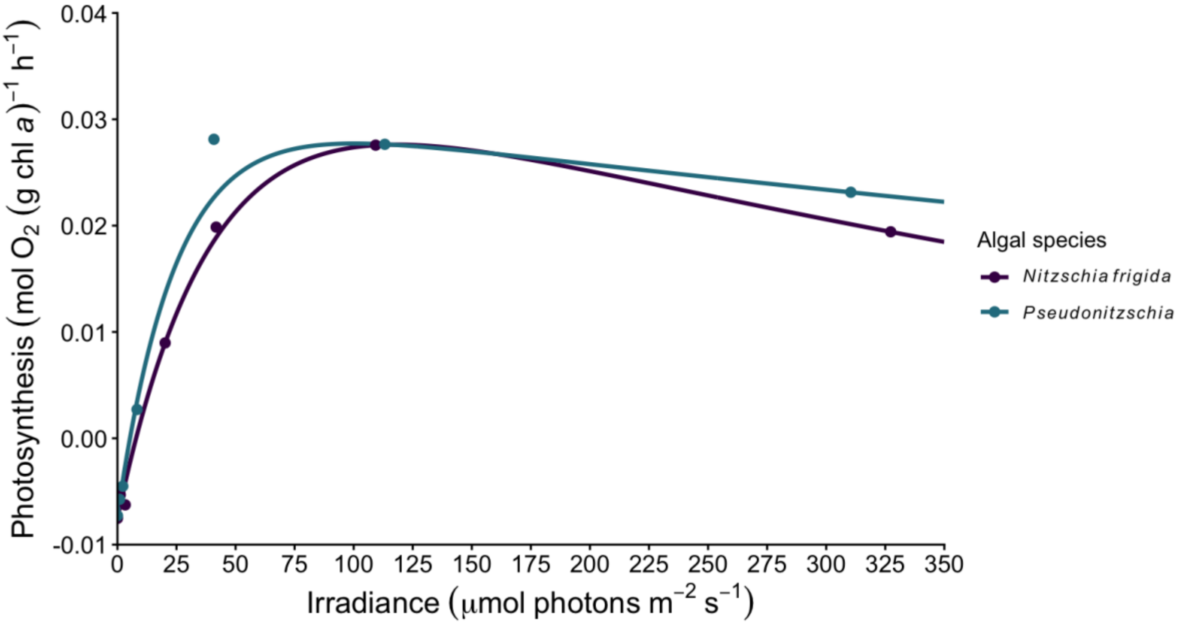

Figure S10: Photosynthesis-Irradiance curves for net community production experiments. Algal species studied were *Nitzschia frigida* (purple) and *Pseudonitzschia sp.* (blue).

Table S3: Carbon and nutrient ratios in the bottom 5 cm ice and sea-water salinity normalized bottom 5 cm ice nutrient concentrations.

Site / ice type	POC:PON	C:N	N:Si	N:P	Si:P	$NO_3 + NO_2$ (µmol l^{-1})	PO4 (µmol l^{-1})	$Si(OH)_4$ (µmol l^{-1})
1 / FYI	6.78	7.91	3.57	4.26	1.19	13.21	3.10	3.70
2 / SYI thick snow	6.25	7.29	9.83	11.66	1.19	22.84	1.96	2.32
2 / SYI thin snow	6.29	7.34	3.29	6.97	2.12	18.62	2.67	5.66
3 / SYI	5.72	6.67	4.86	5.45	1.12	12.95	2.38	2.66

References

Copernicus Climate Change Service (C3S): ERA5: Fifth generation of ECMWF atmospheric reanalyses of the global climate, available at: https://cds.climate.copernicus.eu/ (last access: [1 June 2023]) , 2023.

Hersbach, H., Bell, B., Berrisford, P., Hirahara, S., Horányi, A., Muñoz-Sabater, J., Nicolas, J., Peubey, C., Radu, R., Schepers, D., and others: The ERA5 global reanalysis, Q. J. R. Meteorol. Soc., 146, 1999–2049, https://doi.org/10.1002/qj.3803, 2020.

Lenss, M., Moreau, S., Chierici, M., Claeys, P., Fransson, A., Gerland, S., Itkin, P., Osanen, J., Różańska-Pluta, M., Salganik, E., Wiktor, J., and Campbell, K.: Incorporated platelet ice layers provide refuge for sea-ice algae in the Kong Håkon VII Hav, Mar. Ecol. Prog. Ser., 774, 143–164, https://doi.org/10.3354/meps14979, 2025.

Ocean and Sea Ice Satellite Application Facility (OSI SAF): Global Sea Ice Concentration (netCDF) – DMSP (OSI-401-d) Data extracted from https://thredds. met.no/thredds/dodsC/osisaf/met.no/ice/conc_nh_pol_agg.html (15-05-2023–10-09-

2022) (Northern Hemisphere), EUMETSAT Ocean and Sea Ice Satellite Application Facility, 2017, (accessed 1 June 2023).

Ocean and Sea Ice Satellite Application Facility (OSI SAF): Global Low Resolution Sea Ice Drift – Multimission (OSI-405-c), Data extracted from https://thredds.met. no/thredds/dodsC/osisaf/met.no/ice/drift_lr_nh_agg. html (15-05-2023–10-09-2022) (Northern Hemisphere), EUMETSAT Ocean and Sea Ice Satellite Application Facility, 2010, (accessed 1 June 2023).

Detailed list of species abundance (10^5 cells L^{-1}) in the bottom 0-5 cm of sea ice from the 2023 BREATHE Drift Cruise north of Svalbard following analysis by light microscopy. Taxonomic orders are highlighted in bold, suborders are underlined. Species names have been referenced from the WoRMS Editorial Board (2026). World Register of Marine Species. Available from https://www.marinespecies.org at VLIZ. Accessed 2026-03. doi:10.14284/170

Text S1. Taxonomy of cells over 2 µm in the bottom 5 cm of ice.

Sampling Site	**1**	**2 Thick snow**	**2 Thin snow**	**3**
Sampling date (2023)	19/05/2023	22/05/2023	22/05/2023	27/05/2023
Abundance	10^5 cells L^{-1}	10^5 cells L^{-1}	10^5 cells L^{-1}	10^5 cells L^{-1}
Total abundance	**753.4**	**448.6**	**327.5**	**358.3**
1) Bacillariophyta	653.9	352.1	231.9	276.1
1A) <u>Centric Diatoms</u>	105.4	53.7	40.9	48.3
Attheya spp. (large and distinct), West 1860	7.8	3.3	3.6	2.0
Attheya spp. (small with short hairs)	11.7	13.2	1.4	1.3
Leptocylindrus danicus Cleve 1889	7.8	0.0	0.0	0.0
Centric diatoms spp. (2-10µm)	62.5	28.5	10.8	30.0
Centric diatoms spp. (10-20µm)	15.6	8.8	1.4	0.7
Chaetoceros/Attheya sp. (0-10 um)	0.0	0.0	20.1	13.7
Chaetoceros/Attheya sp. (10-20 um)	0.0	0.0	3.6	0.7
1B) <u>Pennate Diatoms</u>	548.5	298.3	191.0	227.8
Cylindrotheca closterium (Ehrenberg) Reimann & J.C.Lewin 1964	9.8	7.7	7.9	5.2
Entomoneis spp. Ehrenberg, 1845	2.0	0.0	3.6	4.6
Fossula arctica G.R.Hasle, E.E.Syvertsen & C.H.von Quillfeldt, 1996	0.0	0.0	1.4	0.0
Fragilariopsis cylindrus (Grunow) Krieger, 1954	0.0	23.0	8.6	0.0
Fragilariopsis spp.	0.0	0.0	0.0	11.7
Haslea crucigeroides (Hustedt) Simonsen, 1974	0.0	12.1	2.9	7.2
Navicula c.f. directa	0.0	0.0	7.9	13.1
Navicula gelida Grunow, 1884	0.0	0.0	10.8	6.5
Navicula kariana Grunow in Cleve & Grunow, 1880	2.0	0.0	0.0	0.0
Navicula pagophila var. *manitounukensis* Poulin & Cardinal, 1982	0.0	0.0	0.7	0.7
Navicula pelagica Cleve, 1896 (10-20 um)	0.0	1.1	0.0	1.3
Navicula pelagica Cleve, 1896 (20-30 um)	0.0	6.6	2.2	0.0
Navicula transitans Cleve, 1883	0.0	1.1	0.0	0.0
Navicula spp. (20-50µm)	3.9	11.0	2.9	3.9
Navicula spp. (50µm plus)	0.0	2.2	0.7	0.7
Nitzschia frigida Grunow, 1880	181.5	100.9	61.7	39.2
Nitzschia laevissima Grunow in Cleve, 1883	2.0	1.1	0.0	0.7
Nitzschia promare Medlin, 1990	15.6	0.0	5.0	3.9
Nitzschia spp. (20-50µm)	15.6	6.6	10.1	24.2

Nitzschia spp. (50-100 µm)	15.6	7.7	9.3	11.7
Nitzschia spp. (>100um)	3.9	2.2	1.4	0.7
Pseudo-nitzschia delicatissima (Cleve) Heiden, 1928	146.4	26.3	10.8	18.9
Pseudo-nitzschia seriata (Cleve) H.Peragallo, 1899	23.4	0.0	0.0	0.0
Nitzschia seriata f. obtusa Hasle, 1965	29.3	23.0	12.9	30.0
Synedropsis hyperborea (Grunow) G.R.Hasle, L.K.Medlin & E.E.Syvertsen, 1994	15.6	0.0	0.0	1.3
Pennate Diatoms spp. Chain (20-50 um)	0.0	3.3	0.0	0.0
Pennate Diatoms spp. (5-10µm)	15.6	7.7	0.7	7.2
Pennate Diatoms spp. (10-20µm)	31.2	12.1	7.9	17.0
Pennate Diatoms spp. (20-50µm)	33.2	42.8	20.1	18.3
Pennate Diatoms spp. (50µm plus)	2.0	0.0	1.4	0.0
2) Dinophyceae	29.3	31.8	19.4	13.7
Dinophyceae (athecate)	29.3	31.8	19.4	13.7
Gymnodinium/Gyrodinium spp. (5-10µm)	2.0	7.7	6.5	2.0
Gymnodinium/Gyrodinium spp. (10-20µm)	17.6	19.7	10.1	8.5
Gymnodinium/Gyrodinium spp. (20-50µm)	9.8	4.4	2.9	3.3
3) unidentified flagellates	70.3	64.7	75.4	68.5
Flagellates spp. (2-5µm); no distinguishing features	17.6	30.7	17.9	25.5
Flagellates spp. (5-10µm)	35.1	28.5	35.2	30.7
Flagellates spp. (10-20µm)	17.6	5.5	22.3	12.4
5) Ciliophora	0.0	0.0	0.7	0.0
Ciliates spp. (20-50µm)	0.0	0.0	0.7	0.0
6) Others	2.0	0.0	10.8	0.0
Cysts (0-10µm)	0.0	0.0	5.0	0.0
Cysts (10-20µm)	0.0	0.0	5.7	0.0
Cysts (20-50µm)	2.0	0.0	0.0	0.0
Total cells (excluding others)	753.4	448.6	327.4	358.3
Total cells (including others)	755.4	448.6	338.2	358.3